THE JOURNAL OF BIOLOGICAL CHEMISTRY VOL. 290, NO. 30, pp. 18467–18477, July 24, 2015
Published in the U.S.A.

α-Synuclein Shows High Affinity Interaction with Voltage-dependent Anion Channel, Suggesting Mechanisms of Mitochondrial Regulation and Toxicity in Parkinson Disease*

Received for publication, January 28, 2015, and in revised form, June 4, 2015 Published, JBC Papers in Press, June 8, 2015, DOI 10.1074/jbc.M115.641746

Tatiana K. Rostovtseva[‡1], Philip A. Gurnev[‡§2], Olga Protchenko[¶], David P. Hoogerheide[‡‖3], Thai Leong Yap[**], Caroline C. Philpott[¶], Jennifer C. Lee[**], and Sergey M. Bezrukov[‡]

*From the [‡]Program in Physical Biology, Eunice Kennedy Shriver NICHD, National Institutes of Health, Bethesda, Maryland 20892, the [§]Physics Department, University of Massachusetts, Amherst, Massachusetts 01003, the [¶]Liver Diseases Branch, NIDDK, National Institutes of Health, Bethesda, Maryland 20892, the [‖]Center for Neutron Research, National Institute of Standards and Technology, Gaithersburg, Maryland 20899, and the **Laboratory of Molecular Biophysics, NHLBI, National Institutes of Health, Bethesda, Maryland 20892*

Background: The intrinsically disordered protein α-synuclein, a hallmark of Parkinson disease, is involved in mitochondrial dysfunction in neurodegeneration and directly interacts with mitochondria.
Results: α-Synuclein regulates VDAC permeability; α-synuclein toxicity in yeast depends on VDAC.
Conclusion: α-Synuclein both blocks VDAC and translocates via this channel across the mitochondrial outer membrane.
Significance: (Patho)physiological roles of monomeric α-synuclein may originate from its interaction with VDAC.

Participation of the small, intrinsically disordered protein α-synuclein (α-syn) in Parkinson disease (PD) pathogenesis has been well documented. Although recent research demonstrates the involvement of α-syn in mitochondrial dysfunction in neurodegeneration and suggests direct interaction of α-syn with mitochondria, the molecular mechanism(s) of α-syn toxicity and its effect on neuronal mitochondria remain vague. Here we report that at nanomolar concentrations, α-syn reversibly blocks the voltage-dependent anion channel (VDAC), the major channel of the mitochondrial outer membrane that controls most of the metabolite fluxes in and out of the mitochondria. Detailed analysis of the blockage kinetics of VDAC reconstituted into planar lipid membranes suggests that α-syn is able to translocate through the channel and thus target complexes of the mitochondrial respiratory chain in the inner mitochondrial membrane. Supporting our *in vitro* experiments, a yeast model of PD shows that α-syn toxicity in yeast depends on VDAC. The functional interactions between VDAC and α-syn, revealed by the present study, point toward the long sought after physiological and pathophysiological roles for monomeric α-syn in PD and in other α-synucleinopathies.

Emerging evidence establishes the critical role of mitochondria in the pathogenesis of neurodegenerative diseases including Parkinson disease (PD)[4] and Alzheimer disease (1, 2). Dysfunction of mitochondrial enzyme complexes, production of reactive oxygen species, mitochondrial outer membrane (MOM) permeabilization, enhanced apoptosis, and structural alterations of mitochondria have been associated with these pathologies (1–3). Neurons are especially sensitive to mitochondrial dysfunction because of their high demand for energy and their characteristic subcellular distribution of mitochondria. α-Synuclein (α-syn) is a small, intrinsically disordered neuronal protein that is involved in the etiology of PD (4) and various α-synucleinopathies (5). This protein is a major structural component of intracellular protein inclusions, or Lewy bodies, that constitute a pathological hallmark of PD (4). Recent research demonstrates the involvement of α-syn in mitochondrial dysfunction in neurodegeneration and in induction of neuroapoptosis (3, 6–9) and suggests direct interaction of α-syn with mitochondria (6, 7, 9, 10). However, the exact mechanism of α-syn toxicity and its effect on neuronal mitochondria in particular remain elusive. It was shown that α-syn gene mutations cause early onset of PD (11–13). The observation that Lewy bodies are enriched with fibrillar α-syn has led to a hypothesis of the neurotoxicity of fibrillar components (14). Therefore, most of the studies so far have been focused on the role of α-syn aggregates in PD, where α-syn monomers are regarded simply as supplies for the aggregates.

There are three distinctive amino acid regions of α-syn: the membrane-binding amphipathic N-terminal domain (residues 1–60), the mostly hydrophobic central part, also called the non-amyloid β component domain (residues 61–95), and the highly acidic C-terminal tail containing 15 negative charges (residues 96–140) (14). In physiological salt solutions, α-syn

* This work was supported, in whole or in part, by the Intramural Research Program of the National Institutes of Health (NIH), Eunice Kennedy Shriver NICHD, NIDDK, and NHLBI. The authors declare that they have no conflicts of interest with the contents of this article.
[1] To whom correspondence should be addressed: Program in Physical Biology, Eunice Kennedy Shriver NICHD, National Institutes of Health, 9000 Rockville Pike, Bldg. 9, Rm. 1E-106, Bethesda, MD 20892-0924. Tel.: 301-402-4702; Fax: 301-496-2172; E-mail: rostovtt@mail.nih.gov.
[2] Supported by National Science Foundation EAGER Award 1249199.
[3] Recipient of a National Research Council Research Associateship Award at the National Institute of Standards and Technology and the National Institutes of Health.

[4] The abbreviations used are: PD, Parkinson disease; MOM, mitochondrial outer membrane; α-syn, α-synuclein; VDAC, voltage-dependent anion channel; FL, full-length; ROS, reactive oxygen species; PT, permeability transition; ANT, adenine-nucleotide translocator.

exists in an intrinsically disordered form (15). When α-syn binds to the negatively charged lipid membranes, the N terminus adopts a helical form, and the acidic C terminus remains unstructured and does not interact with the membrane (16). Interestingly, it was also found that α-syn preferentially interacts with mitochondrial membranes compared with other native cell membranes, such as endoplasmic reticulum or plasma membranes (17), and the specificity of α-syn binding to the mitochondrial membranes does not depend on the functional state of mitochondria. However, another group (6) reported that import of human α-syn to mitochondria under *in vivo* and *in vitro* conditions depends on the mitochondrial membrane potential and mitochondrial ATP level. It was shown that α-syn is predominantly associated with the inner mitochondrial membrane in human dopaminergic neurons (6) and HEK cells (18) and that accumulation of α-syn in mitochondria impairs complex I of the mitochondrial electron transport chain inducing oxidative stress. Other groups reported accumulation of α-syn on the MOM of mouse brain (10) or HEK cells (19) but the absence of the inhibition effect of α-syn on complex I (8). Therefore, questions regarding α-syn localization in mitochondria, the mechanism underlying selective α-syn binding to the mitochondrial membranes, and the role of mitochondrial bioenergetics in the α-syn interaction with mitochondria remain open. Notably, most studies agree on the inhibitory effect of α-syn on the mitochondrial oxidative phosphorylation capacity and on the promotion of oxidative stress.

Surprisingly, there have been no serious attempts to identify the pathway(s) for the translocation of water-soluble α-syn across the MOM from the cytosol to the mitochondrial inner membrane, although the latest reports suggest that α-syn can bind to voltage-dependent anion channel (VDAC), the main channel in the MOM. Lu *et al.* (20) showed that α-syn overexpressed in the substantia nigra of rats co-immunoprecipitated with VDAC. Human A53T-mutant α-syn associated with dysmorphic neuronal mitochondria also co-immunoprecipitated with VDAC in the brainstem, striatum, and cortex of early and late symptomatic human α-syn transgenic mice (9). These reports raise the possibility that VDAC, a large β-barrel channel suitable for transport of metabolites and polypeptides, could be a pathway for α-syn translocation into the mitochondria.

VDAC controls a significant portion of the outer membrane function (21–24). Because VDAC has been shown to be involved in a wide variety of mitochondria-associated pathologies, including neurodegenerative disorders, such as PD, Alzheimer disease, and amyotrophic lateral sclerosis, VDAC is emerging as a promising pharmacological target (25). This multifunctional channel is regarded as a conjunction point for a variety of cell signals mediated by various cytosolic proteins (26–28). Any restriction to the metabolite exchange through VDAC affects the mitochondrial functions.

Here, we study the functional interaction of α-syn with VDAC reconstituted into lipid bilayers and find that nanomolar concentrations of recombinant monomeric α-syn reversibly block VDAC in a highly voltage-dependent manner. Furthermore, a detailed kinetic analysis of the blockage events suggests that α-syn is able to translocate through VDAC. Experiments with a yeast strain deficient in *VDAC1* (*por1*Δ) demonstrate that α-syn toxicity in yeast depends on VDAC, revealing an α-syn interaction with VDAC in living cells. Considering that VDAC is a major conduit for respiratory substrates across the MOM, our results suggest that the functional interaction of monomeric α-syn with VDAC could be essential for both physiological adaptation of mitochondrial respiration and dysfunction in PD and other α-synucleinopathies.

Experimental Procedures

Protein Purification—VDAC was isolated from frozen mitochondrial fractions of rat liver that were a generous gift of Dr. Marco Colombini (University of Maryland, College Park, MD) and purified following the standard methods (29). WT α-syn full-length (FL) was expressed, purified, and characterized as described previously (30). Purified protein was buffer-exchanged (20 mM Tris and 0.1 M NaCl, pH 8), using Amicon Ultra-15 centrifugal filter units (molecular mass cut-off 3 kDa; Millipore) and stored at −80 °C. Protein concentrations were determined using an extinction coefficient of 5120 M^{-1} cm^{-1} at 280 nm using a Cary 300 biospectrophotometer (Varian). Plasmid for α-syn carrying residues 1–115 (α-syn N115) was constructed using the QuikChange site-directed mutagenesis kit (Stratagene) through insertion of a stop codon. Mutation was verified by DNA sequencing. Mutant α-syn N115 was expressed, purified, and characterized as described previously (31). α-Syn mutants A53T and A30P and the C terminus peptide corresponding to residues 96–140 of α-syn (C45) were purchased from rPeptide (Bogart, GA).

Channel Reconstitution—Planar bilayer membranes were formed from diphytanoyl-phosphatidylcholine (Avanti Polar Lipids, Alabaster, AL), and channel currents were analyzed as described previously (31, 32). VDAC insertion was achieved by adding purified VDAC in a 2.5% Triton X-100 solution to the aqueous phase of 1 M (1 mol/liter) KCl buffered with 5 mM Hepes at pH 7.4 in the *cis* compartment while stirring. Potential is defined as positive when it is greater at the side of VDAC addition (*cis*). α-Syn was added to the membrane-bathing solutions after VDAC channel reconstitution; statistical analysis of the blockage events was started 15 min after the α-syn addition to ensure a steady state.

Analysis of Open and Blocked Times—Blockage events were identified using a threshold detection algorithm implemented with custom MATLAB (Mathworks) code. The absolute values of the current traces were median-filtered (order 3) and compared with a threshold equal to 80% of the open pore current. The times at which each threshold crossing occurred were recorded and designated as "positive" or "negative" based on the slope of the current at the threshold crossing. Histograms of τ_{on} were compiled on a logarithmic scale from the intervals between each positive threshold crossing and the subsequent negative threshold crossing. Histograms of τ_b were compiled on a logarithmic scale from the intervals between each negative threshold crossing and the subsequent positive threshold crossing. Each distribution bin was weighted by Poisson statistics and fit to an exponential function (33) using a Levenburg-Marquardt algorithm. Unless otherwise stated, error bars are calcu-

lated from bootstrap distributions obtained by random resampling of the experimentally observed time distributions.

Yeast Strains, Plasmids, and Media—*Saccharomyces cerevisiae* BY4742 (*MATα his3Δ1 leu2Δ0 lys2Δ0 ura3Δ0*) and *por1*Δ (ATCC) strains were used in this study. Plasmid pESC-SYN (34) was a kind gift from Dr. F. Madeo (University of Graz, Graz, Austria), and plasmid pYX212-hVDAC1 (35) was a kind gift from Dr. Vito DePinto (University of Catania, Italy). Transformants were selected and grown on synthetic complete (SC) media lacking uracil and histidine. SC media were prepared as described elsewhere (36). 2% glucose (non-inducing media) or 2% galactose (inducing media) were used as carbon sources. Yeast were washed and resuspended in water at OD = 1 and then subjected to serial 10-fold dilution. Yeast were spotted in 10-μl volumes, allowed to dry, and then grown at 30 or 37 °C for 3 days. Plates were imaged, and growth was quantitated from the scanned image using Adobe Photoshop version CS5.1 by measuring the sum of pixel intensity of the yeast spot less an equal area of medium without yeast.

Western Blotting—Strains were pregrown in SC medium supplemented with 2% raffinose (non-inducing condition) at 30 °C and inoculated for overnight growth in SC medium with 2% galactose at 37 °C. Cell lysates were prepared as described (37). Briefly, cells were harvested by centrifugation, washed in double-distilled H_2O. Cells were resuspended in 1× LDS sample buffer (Invitrogen) with 2.5% β-mercaptoethanol with the protease inhibitor mixture (Roche Applied Science) and boiled for 5 min. Samples were run on 4–12% SDS-PAGE (Invitrogen) and blotted onto a PVDF membrane. α-Syn-FLAG was detected using a mouse monoclonal anti-FLAG antibody (Sigma) and anti-mouse IRDye 800RD secondary antibodies (LI-COR Biosciences). Human VDAC1 was detected using a rabbit polyclonal anti-VDAC1 antibody (Millipore), anti-rabbit HRP-conjugated secondary antibodies (Jackson Immunoresearch), and enhanced chemiluminescence substrate (Pierce).

Results

α-Syn Reversibly Blocks VDAC Reconstituted in Planar Lipid Bilayers—Ion channel reconstitution is so far the best available method for direct functional studies of organelle channels, such as mitochondrial VDAC. When reconstituted into planar lipid membranes, VDAC forms large, 4-nanosiemens (in 1 M KCl) anion-selective channels permeable for non-charged polymers up to a few kDa (38–40) and for ATP (29, 42). Depending on experimental conditions, such as lipid composition and salt concentration, the channel can stay open for a few seconds even at an applied voltage as high as 60 mV. The addition of nanomolar concentrations of α-syn to the membrane-bathing solution changes VDAC behavior dramatically. A representative experiment is shown in Fig. 1*A*, where the addition of 50 nM α-syn to a single VDAC causes time-resolved reversible blockages of the channel conductance (*right traces*). α-Syn induces two distinct blocked states, depending on its concentration and the applied voltage. The first blocked state (B1) is characterized by a conductance of ~40% that of the open state (Fig. 1*A*, *a*). A second, deeper blocked state (B2) with a conductance of ~17% that of the open state is observed at potentials $|V| \geq 30$ mV (Fig. 1*A*, *b* and *c*); the incidence of this state increases with the applied voltage (event amplitude histograms in Fig. 1*A*, *a–c*). α-Syn blocks VDAC from both sides of the channel, but only when a negative potential is applied from the side of the α-syn addition, suggesting that the negatively charged C-terminal region of α-syn is responsible for the observed VDAC blockage.

The distribution of times between blockage events when the channel is open, τ_{on}, is well described by a single exponential function at all applied potentials (Fig. 1*C*, *a*). The on-rate of the blockage, $\langle\tau_{on}\rangle^{-1}$, is highly voltage-dependent (Fig. 1*B*, *top*). The blockage is adequately described as a first-order binding reaction with the on-rate first increasing proportionally to the α-syn concentration, followed by saturation at ~50 nM α-syn (Fig. 2*A*). The characteristic time the channel spends in the blocked state, $\tau_{off} = \langle\tau_b\rangle$, calculated at 25 mV, where only B1 is observed (see Fig. 1*A*, *a*), is virtually independent of the α-syn concentration (Fig. 2*A*, *inset*). The voltage dependence of the equilibrium constant of α-syn binding to VDAC, K_{eq}, defined as $\tau_{off}/(\langle\tau_{on}\rangle C)$, where C is the bulk concentration of α-syn, spans 6 orders of magnitude and, at voltages between −40 and −15 mV, can be fit with an effective "gating charge" of 11.4 ± 1.4 (*solid line* in Fig. 2*B*).

In order to analyze binding kinetics at α-syn concentrations well below saturation, a series of experiments were performed at 1 nM α-syn. Representative traces in Fig. 3*A* demonstrate that at 1 nM, the number of blockage events is dramatically reduced compared with 50 nM (*traces a–c* in Figs. 1*A* and 3*A* obtained at the same voltages). The on-rates are also highly voltage-dependent (Fig. 3*B*, *top*) and can be approximated by exponential dependences.

Interestingly, at 1 nM α-syn, B2 is only observed at the high applied voltage of −60 mV (Fig. 3*A*, *d*). The distributions of blockage times τ_b are adequately described by single exponents for all voltages at 1 nM α-syn (Fig. 3*C*) or when the probability of B2 is relatively small compared with that of B1 at 50 nM α-syn (Fig. 1*C*, *b*). At 50 nM α-syn for $|V| \geq 45$ mV, when the probability of B2 becomes comparable with the probability of B1 (event amplitude histogram in Fig. 1*A*, *c*), a single exponent no longer satisfactorily describes the histogram of τ_b (Fig. 1*C*, *c*). A two-exponential fit of the blockage time histogram (*dashed line* in Fig. 1*C*, *c*) fits long-time events satisfactorily but not the short-time blockages.

The exponential increase of τ_{off} with voltage at $|V| \leq 43$ mV suggests that the mechanism of α-syn blockage of VDAC, similarly to that of tubulin (27), is a reversible block (Fig. 4). At higher potentials, however, the voltage dependence of τ_{off} changes dramatically, and τ_{off} begins to decrease with voltage. The decrease is better seen when τ_{off} is plotted on a linear scale (*bottom panels* in Figs. 1*B* and 3*B*), whereas the exponential increase of τ_{off} at lower applied voltage is more evident on a logarithmic scale (*middle panels* in Figs. 1*B* and 3*B*). The decrease of the residence time at high voltages is seen in Fig. 3*C* as a shift of the blockage time distribution at −60 mV toward shorter times compared with that at −45 mV. The traditional interpretation of this decrease is a voltage-driven translocation (31, 43–47), so that the biphasic behavior of the residence time voltage dependence suggests translocation of α-syn through the VDAC pore (Fig. 4).

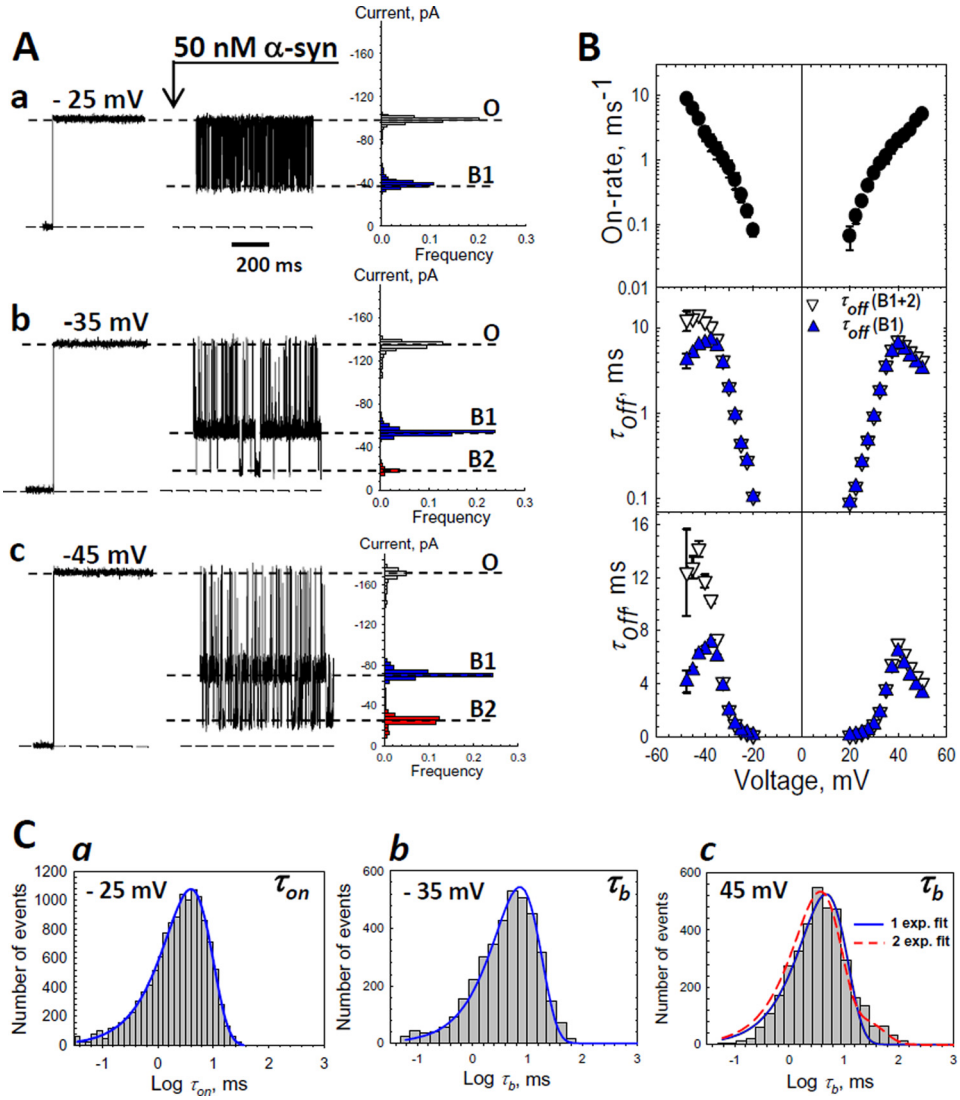

FIGURE 1. **VDAC is reversibly blocked by α-syn in nanomolar concentrations.** *A*, representative traces of ion currents through the single VDAC channel before (*left*) and after (*right*) the addition of 50 nM α-syn to the both sides of the membrane at the indicated voltages. Time-resolved blockage events are characterized by two well defined conducting states, "blocked state 1" (*B1*) and "blocked state 2" (*B2*), with B2 seen at $|V| \geq 30$ mV. The event amplitude histograms show that the relative probability of B2 increases with voltage. The *dashed lines* indicate open (*O*) and blocked (*B1* and *B2*) conductance states and zero current. The membrane-bathing solution contained 1 M KCl buffered with 5 mM HEPES, pH 7.4. Current records were additionally filtered using a 5-kHz 8-pole digital Bessel filter. *B*, voltage dependences of the on-rate of α-syn blockage, $\langle\tau_{on}\rangle^{-1}$, in the presence of 50 nM α-syn (*top panel*) and of the residence time, $\tau_{off} = \langle\tau_b\rangle$, where τ_b is the time of the blockage event. The residence time is presented in both logarithmic (*middle panel*) and linear (*bottom panel*) scales. $\tau_{off}^{(B1)}$ was calculated as the average time at the first blocked conductance level; $\tau_{off}^{(B1+B2)}$ gives the average time in the blocked states without discrimination between the two states. *Error bar*, S.E. *C*, corresponding log-binned distributions (33) of the open time, τ_{on}, at −25 mV (*a*) and of the time of the blockage events, τ_b, calculated for both closed states (B1 + B2) at −35 mV (*b*) and 45 mV (*c*) from statistical analysis of the current records at 50 nM α-syn such as those shown in *A*. *Solid lines*, logarithmic single exponential fittings with characteristic times $\langle\tau_{on}\rangle$ equal to 3 ± 0.1 ms (*a*) and $\langle\tau_b\rangle$ equal to 6.5 ± 0.1 ms (*b*) and to 4.7 ± 0.1 ms (*c*). A two-exponential fit of the blockage time histogram (*dashed line*) at 45 mV (*c*) with characteristic times of 3.5 and 22.1 ms fits the long-time events satisfactorily but not the short-time blockages.

To rule out the possibility that at higher α-syn concentrations, the residence time in B1, $\tau_{off}^{(B1)}$, decreases with voltage due to the increasing probability of B2, we analyzed separately $\tau_{off}^{(B1)}$ and all blockage events, including both states (B1 + B2), $\tau_{off}^{(B1+B2)}$ (*two bottom panels* in Fig. 1*B*). The difference between $\tau_{off}^{(B1)}$ and $\tau_{off}^{(B1+B2)}$ is seen at $|V| \geq 43$ mV, where the contribution of the second blocked state becomes significant, with $\tau_{off}^{(B1+B2)}$ higher than $\tau_{off}^{(B1)}$. However, both residence times show a pronounced decrease at $|V| \geq 43$ mV. Therefore, the decrease in $\tau_{off}^{(B1)}$ at high applied voltages at 50 nM α-syn cannot be explained by the contribution from the second blocked state.

In the two experiments presented in Figs. 1 and 3, α-syn was added to both compartments. Therefore, when the potential is positive, it drives the anionic C terminus of α-syn in the *trans* compartment to the pore, and, *vice versa*, when the potential is negative, it acts on the α-syn terminus in the *cis* compartment.

To test the suggested importance of the negatively charged C-terminal tail of α-syn for VDAC blockage, we performed experiments with a mutant α-syn N115 (amino acids 1–115) in which the last 23 amino acids representing about half of the C-terminal region were truncated. The ability of this mutant to block VDAC was strongly reduced. Fig. 5*A* illustrates that 100

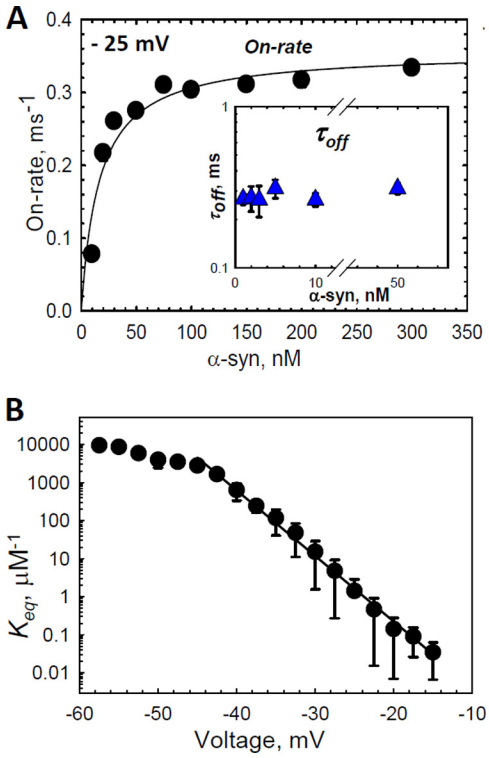

FIGURE 2. **VDAC blockage depends on α-syn concentration and on applied voltage.** *A*, on-rate of the VDAC blockage increases with the α-syn concentration and saturates, whereas the residence time (*inset*) is virtually concentration-independent. The *solid line* is a fit by a simple binding isotherm, yielding K_d = 16.4 ± 1.0 nM. Data were collected at $V = -25$ mV. *B*, equilibrium constant of α-syn binding to VDAC, K_{eq} is highly voltage-dependent. The data are mean values obtained in five independent experiments ± S.E. (*error bars*) at 1, 2, 3, 5, 10, and 50 nM α-syn. τ_{off} was calculated for the B1 + B2 level. Other experimental conditions are as in Fig. 1. The *solid line* is a fit to $K_{eq}(V) = K_{eq}(0)\exp(n|V|e/kT)$, where V is the applied voltage and n is the effective "gating charge" of 11.4 ± 1.4, with e, k, and T having their usual meaning of the elementary charge, Boltzmann constant, and absolute temperature, respectively.

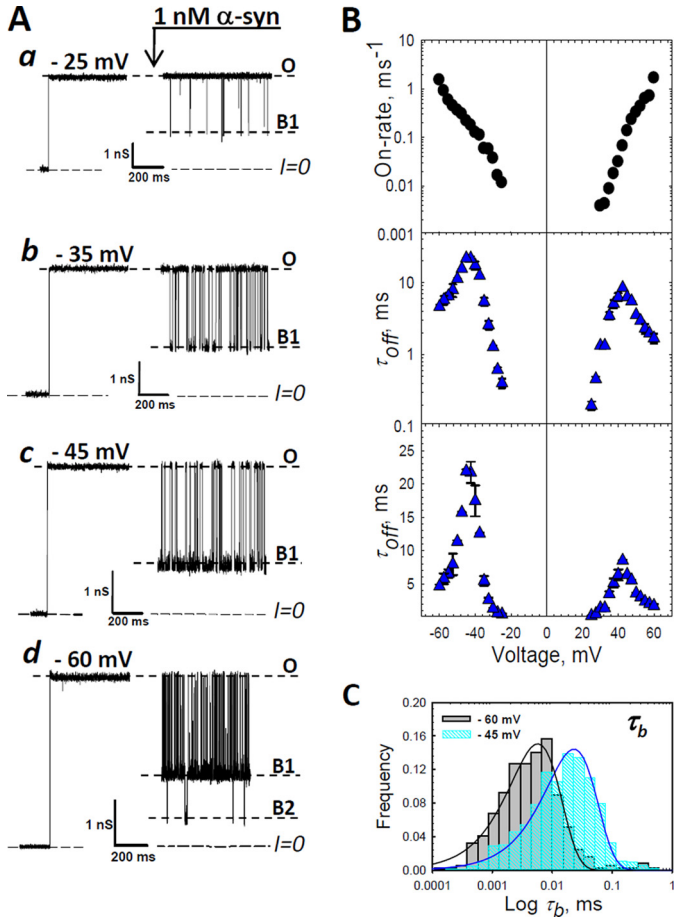

FIGURE 3. **Kinetics of VDAC blockage by α-syn at concentrations below saturation.** *A*, traces of the current through the same single VDAC channel before (*left*) and after (*right*) the addition of 1 nM α-syn to both sides of the membrane at the indicated voltages. Other experimental conditions are as in Fig. 1. *B*, kinetic parameters of VDAC blockage by α-syn, the on-rate (*top panel*) and the residence time, are highly voltage-dependent. The residence time is shown in both logarithmic (*middle panel*) and linear (*bottom panel*) scales. *Error bars*, S.E. *C*, decrease in the time of the blockage events at $|V| \geq 43$ mV is seen as a shift of log-bin histograms of τ_b obtained at 1 nM α-syn at −45 and −60 mV and fitted by single exponents (*solid lines*) with characteristic times equal to 21.9 ± 0.3 ms and 4.6 ± 0.3 ms, respectively.

nM α-syn N115 starts to induce rare blockage events only at the elevated voltage of 40 mV (*top trace*). This is in striking contrast with α-syn FL, which, already at 50 nM, induces a massive VDAC blockage at a lower voltage of 20 mV (Fig. 5*A*, *bottom trace*). At the same time, a C-terminal peptide, C45, consisting of the last 45 amino acids of α-syn (amino acids 96–140) did not have a measurable effect on VDAC up to 500 nM (Fig. 5*B*, *top trace*) even at 45 mV of applied voltage. When 50 nM α-syn FL was added to the *cis* compartment following the C45 addition, it induced typical VDAC blockages (Fig. 5*B*, *bottom trace*), confirming that the channel was fully functioning and that C45 could not block the channel. These experiments demonstrate that the C terminus of α-syn is essential but not sufficient for VDAC blockage. The N terminus of α-syn, which binds to the lipid membranes in a form of an α-helical conformation (16) is also required for this interaction.

A53T and A30P α-syn mutations were identified in rare familial cases of PD (11, 48) and are located in the N-terminal region of α-syn. Therefore, it seemed reasonable to test both mutants for their interaction with VDAC. It turned out that both A53T and A30P mutants induced VDAC blockage similar to the WT. Kinetic analysis of the on-rates and the residence times of VDAC blockage induced by a 50 nM concentration of both mutants in comparison with α-syn WT is shown in Fig. 6. The lack of an effect of physiologically important mutations in the N-terminal domain on both the on- and off-rates of α-syn interaction with VDAC supports our model (Fig. 4) in which the negatively charged C terminus plays an essential role in VDAC blockage.

It is well accepted that the major function of VDAC is to transport and regulate ATP and ADP fluxes across the MOM. ATP permeates through the VDAC open state but not its voltage-induced "closed" state (29). Blockage by α-syn decreases the open channel conductance to a similar extent as the voltage-induced VDAC closure, by ~60% (B1) or ~83% (B2). This suggests that α-syn creates a steric obstruction for ATP and ADP translocation through the VDAC pore. The permeability ratios for Cl^- and K^+ ions, P_{Cl}/P_K, measured in a 1.0 M *cis versus* 0.2 M *trans* KCl gradient are 1.0 ± 0.2 and 1.3 ± 0.3 (mean values ± S.E. of three experiments) for B1 and B2, respectively. Thus, B1 is essentially non-selective, and the selectivity of B2 is

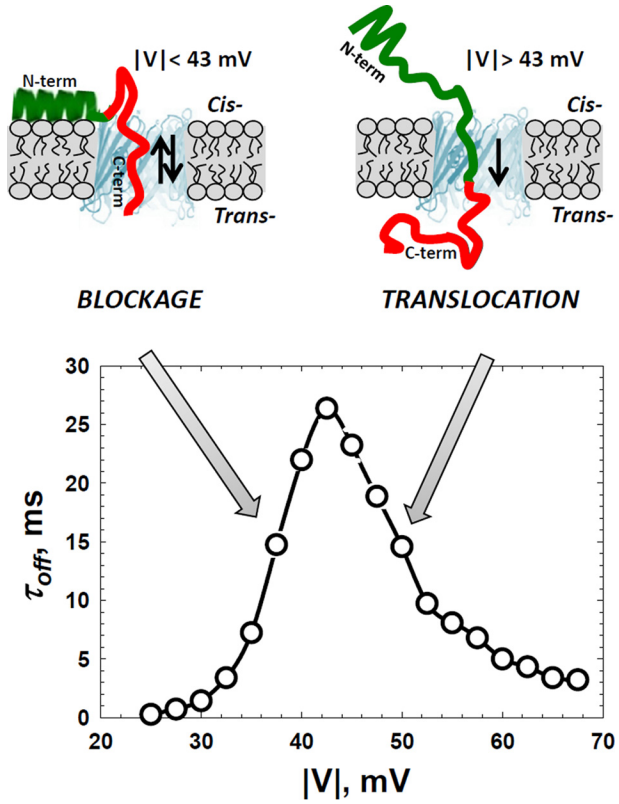

FIGURE 4. **The cross-over in the voltage dependence of the residence time separates regimes of reversible blockage and protein translocation through the pore.** Depending on the amplitude of the applied voltage, α-syn either reversibly blocks ($|V| < 43$ mV) or translocates through ($|V| > 43$ mV) the pore. At the relatively low voltages, upon capture by the channel, an increasing field pulls on the negatively charged C terminus with a force that is not enough to detach the helical part of α-syn from the membrane surface (*N-term; indicated in green*). This results in a reversible capture of the C terminus (*C-term*; indicated in *red*) and in an exponential increase of its residence time in the pore (τ_{off}) with the (absolute) voltage. Voltages that, by amplitude, are above a certain threshold (~43 mV), are high enough to induce detachment of the helical part and drag the whole peptide chain through the pore. In this translocation regime, the increasing field threads protein through the pore faster, which results in the decrease of the residence time. Data points in the graph are the same as in Fig. 3*B* (*bottom panel*), at negative potentials.

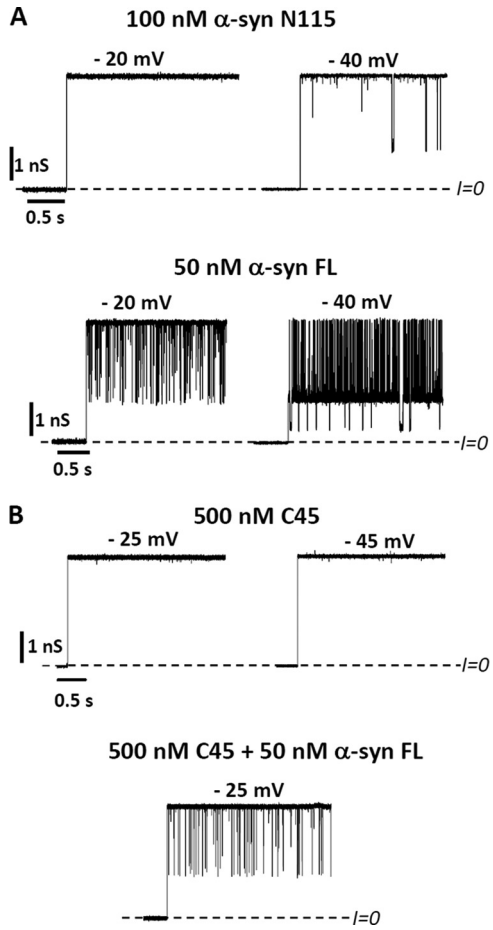

FIGURE 5. **Negatively charged C-terminal tail of α-syn is essential for the efficient blockage.** *A*, representative single channel current traces in the presence of 100 nM α-syn N115 mutant with the truncated C terminus (*top trace*) and 50 nM α-syn FL (*bottom trace*) at 20 and 40 mV of applied voltage. *B*, C terminus peptide of α-syn C45 (residues 96–140) does not block VDAC up to 500 nM concentration (*top trace*) at −25 and −45 mV of applied voltage. When 50 nM α-syn FL was added to the same channel following 500 nM C45 addition, the typical blockage events were observed (*bottom trace*). Other experimental conditions were as in Fig. 1.

only modestly reduced from the open state selectivity characterized by a permeability ratio $P_{Cl}/P_K = 1.5 \pm 0.1$.

It was reported that at concentrations of 140–700 nM, α-syn could form pores in the planar membranes, but only in the presence of the negatively charged or nonlamellar lipids (49). In our control experiments without VDAC, a pore formation activity of α-syn has never been observed in neutral diphytanoyl-phosphatidylcholine membranes used in our experiments and at α-syn concentrations up to 300 nM.

Yeast Model of α-Syn Cytotoxicity—Experiments with reconstituted VDAC demonstrate that α-syn efficiently blocks the VDAC pore, obstructing ADP/ATP exchange between mitochondria and the cytosol. The biphasic character of the residence time voltage dependences also suggests that α-syn translocates through the channel, which could lead to α-syn targeting of the protein complexes of the electron transport chain in the mitochondrial inner membrane. Therefore, it is natural to ask whether these *in vitro* results are relevant to the α-syn toxicity in living cells. To answer this question, we used a yeast model of PD in which human α-syn is expressed in *S. cerevisiae*, which does not contain an endogenous homolog of α-syn. We introduced plasmids carrying α-syn (controlled by an inducible promoter), human VDAC1 (controlled by a strong constitutive promoter), or empty vectors into the wild type BY4742 strain (Fig. 7, *A* and *B*) or the congenic *por1*Δ strain, which lacks the endogenous major VDAC (Fig. 7, *C* and *D*). Plasmid-transformed strains were plated in serial 10-fold dilutions on medium supplemented with galactose (inducing conditions, α-syn expressed) or glucose (repressing conditions, α-syn not expressed) and grown at 37 °C or 30 °C for 3 days. Wild type yeast with or without hVDAC1 alone grew well on galactose medium (Fig. 7*A*, *lanes 1* and *4*). In contrast, wild type yeast expressing α-syn alone grew slowly on galactose (*lane 1 versus lane 2*), and yeast expressing both hVDAC and α-syn exhibited a strong inhibition of growth on galactose (*lane 3*). All plasmid-transformed, wild type yeast grew equally well on glucose, indicating that growth differences between strains were due to plasmid-encoded gene expression and not due to unequal plating. Western blot analysis confirmed the expression of α-syn and hVDAC1 (at low levels) in yeast (Fig. 7*B*).

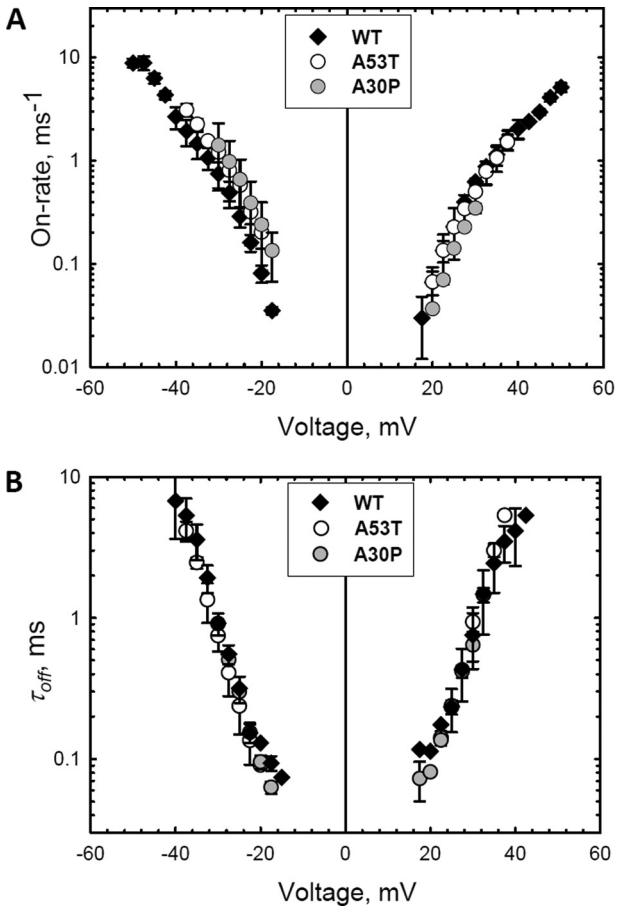

FIGURE 6. **α-Syn mutations A53T and A30P do not affect VDAC blockage.** Voltage dependences of the on-rates and the residence times for α-syn WT and two mutants, A53T and A30P. Synucleins were added to both sides of the membrane at 50 nM concentrations. Data are mean values obtained in 2–3 independent experiments ± S.E. (*error bars*). Experimental conditions were as in Fig. 1.

In contrast to the wild type strain, expression of α-syn alone in the *por1*Δ strain, which lacks the major endogenous VDAC, did not cause slowed growth on galactose medium (Fig. 7*C*, *lanes 1* and *2*). Expression of high levels of hVDAC in the *por1*Δ strain led to moderate inhibition of growth, both on glucose and galactose (*lanes 3* and *4*), but co-expression of both α-syn and hVDAC in the *por1*Δ strain led to a very strong inhibition of growth on galactose (*lane 3*). Again, Western blotting confirmed expression of both exogenous genes in the *por1*Δ strain (Fig. 7*D*). Together, these data indicated that co-expression of α-syn and VDAC (either yeast or human) produced cytotoxicity and that the toxic effects of α-syn were absent in yeast lacking VDAC. This genetic interaction between α-syn and VDAC is consistent with a physical interaction between the two proteins in cells.

Discussion

To summarize, we propose a model of α-syn interaction with VDAC, in which the negatively charged C terminus of α-syn enters the net positive VDAC (Fig. 4). At small applied voltages, the C terminus moves back and forth, with the α-helical bundle of the N terminus bound to the membrane, thus preventing translocation and increasing the residence time of the C terminus inside the pore (Fig. 4). This mechanism is similar to that suggested for the effect of tubulin's negatively charged C-terminal tails on VDAC (50). However, contrary to the findings with tubulin, at $|V| > 43$ mV, the driving force of the applied potential acting on the negatively charged C terminus is large enough to detach the helical N-terminal part of α-syn from the membrane surface and allow the whole molecule to translocate through the channel. Based on the finding that the probability of the second blocked state, B2, increases with α-syn concentration faster than that of the first blocked state, B1, (compare traces at 50 and 1 nM in Figs. 1*A* and 3*A*), we suggest that B2 is not a signature of translocation through the pore (51) but rather is a result of a second α-syn molecule interacting with the pore when the first molecule is already there. The internal dimension of the VDAC pore of ~2.7 nm in its narrowest part (52) is sufficient to accommodate two disordered polypeptides.

A propensity of α-syn for aggregation in solution and at membrane surfaces is well known (16, 53), but aggregation is unlikely under our experimental conditions. α-Syn aggregation in solution occurs at orders of magnitude higher concentrations (hundreds of μM) (54) than those that have been used in our experiments (tens of nM). It was shown that the presence of the negatively charged lipid is a requirement for α-syn aggregation at the membrane surface (16, 55) and that there is no noticeable aggregation at concentrations below tens of μM (56). These results suggest that a likelihood of measurable aggregation of α-syn at the surface of neutral membrane (diphytanoylphosphatidylcholine) and at a 1–100 nM concentration range of α-syn is negligibly low. The same is true for the C terminus-truncated α-syn N115. It was shown in a number of publications (*e.g.* Refs. 54, 57, and 58) that C-terminal deletion increases aggregation in comparison with α-syn WT. However, the aggregation could be achieved only at concentrations of 100–700 μM truncated α-syn, orders of magnitude higher than the concentrations used in our experiments and only under conditions of constant shaking for 1–3 days at 37 °C (57). Serpell *et al.* (54) reported that the minimal concentration for the assembly of the C terminus-truncated human α-syn is 50 μM, which is still well above concentrations that have been used in our work. Thus, in our experiments, α-syn exists in a predominantly monomeric form.

The kinetic analysis of α-syn binding to VDAC suggests at least two physiological consequences for mitochondrial function (Fig. 8). First, α-syn sterically blocks the VDAC pore and thus obstructs fluxes of ATP and ADP across the channel. This leads to a depletion of the electron transport chain complexes of cytosolic ADP, inducing dissipation of the mitochondrial transmembrane potential (59), and eventually to a decrease of oxidative phosphorylation. Likewise, the reversible blockage of VDAC by α-syn may constitute a regulation mechanism of normal mitochondrial respiration in neurons through the modulation of VDAC permeability, pointing to a non-pathological function of monomeric α-syn. This could be a step forward in understanding the involvement of endogenous α-syn in maintaining normal mitochondrial bioenergetics, which is currently an open question (6, 60). Second, our data suggest that VDAC is able to serve as a pathway for α-syn into the intermembrane space, which may result in its direct interaction with the elec-

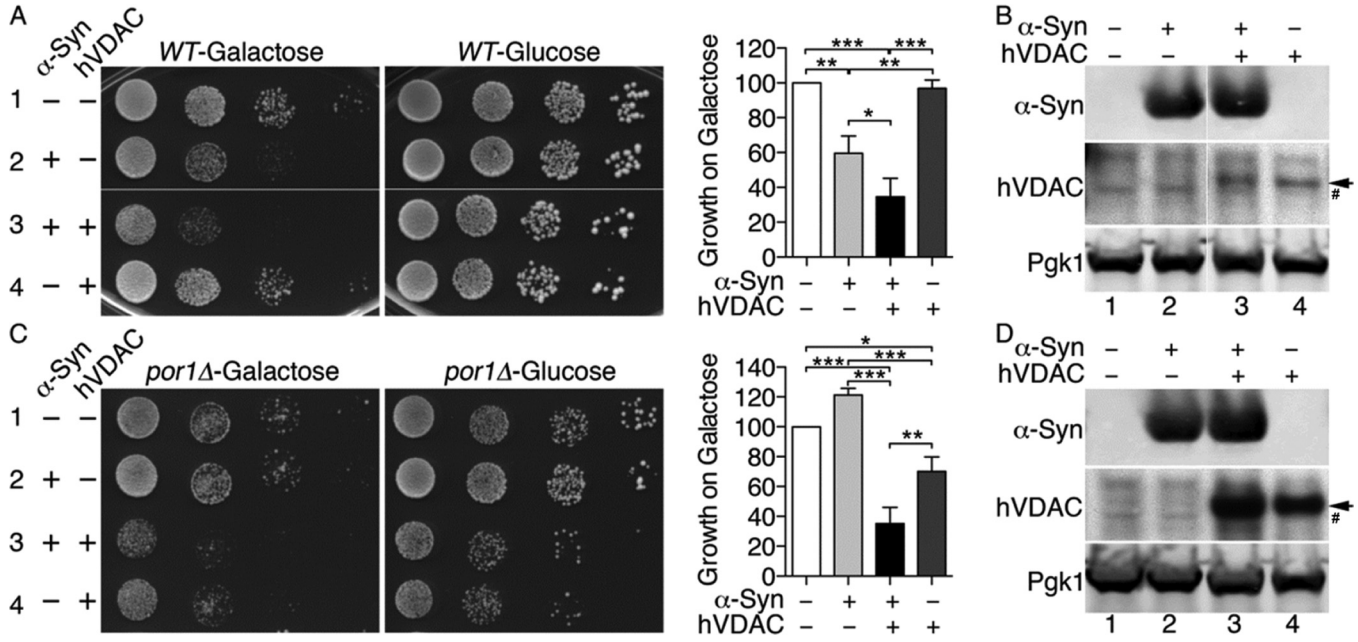

FIGURE 7. **VDAC is required for α-syn cytotoxicity in the yeast model of PD.** *A* and *B*, enhanced toxicity of α-syn in yeast coexpressing human VDAC1. Shown is wild type *S. cerevisiae* strain BY4741 (WT) was transformed with plasmids expressing α-syn (from the galactose-inducible *GAL1,10* promoter) and hVDAC1 (from the constitutive *TPI1* promoter) (+) or empty vectors (−). Plasmid-transformed yeast were plated in serial 10-fold dilutions on medium supplemented with galactose (inducing conditions, α-syn expressed) or glucose (repressing conditions, α-syn not expressed). Plates were grown at 37 °C for 3 days. Growth was quantitated by measuring pixel intensity of yeast images and expressed as a percentage of growth of the strain transfected with empty vectors. The assay was replicated four times. Data were analyzed by one-way analysis of variance ($p = 0.0002$, $R^2 = 0.87$) followed by a Bonferroni multiple comparison test. Here and in *C*, *, $p < 0.05$; **, $p < 0.01$; ***, $p < 0.001$; all significant comparisons are shown. *B*, cells from *A* were analyzed by Western blot. *C* and *D*, loss of α-syn cytotoxicity in yeast without VDAC. A yeast strain deleted for the major mitochondrial VDAC (*por1*Δ) was transformed with plasmids expressing α-syn or hVDAC1 and plated as in *A*. Plates were grown for 3 days at 30 °C. Growth was quantitated as in *A*. The assay was replicated four times. Data were analyzed by one-way analysis of variance ($p < 0.0001$, $R^2 = 0.92$) followed by a Bonferroni multiple comparison test. *D*, Western blot analysis of cells from *C*. Pgk1 was used as a loading control. *Arrow*, hVDAC1; #, nonspecific band. *Error bars*, S.E.

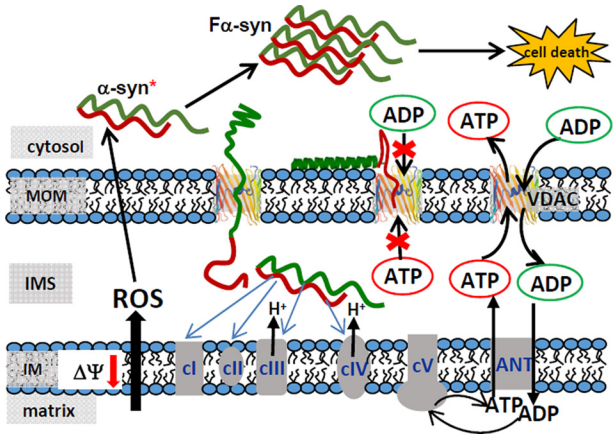

FIGURE 8. **A model of MOM permeability regulation and α-syn-induced cytotoxicity based on α-syn interaction with and translocation through VDAC.** VDAC blockage by α-syn disrupts ATP/ADP exchange between mitochondria and the cytosol, thus distorting the substrate balance for the ANT positioned in the inner membrane (*IM*). This results in the depletion of ATP-synthase (*cV*) with ADP, decreased mitochondrial potential (ΔΨ), and impaired oxidative phosphorylation. By crossing the MOM through VDAC into the intermembrane space (*IMS*), α-syn is able to directly target complexes of the electron transport chain (*cI*, *cII*, *cIII*, and *cIV*) in the inner membrane. This leads to mitochondrial dysfunction characterized by enhanced production of the ROS. In turn, ROS induces monomeric α-syn oxidation (*α-syn**) in the cytosol, causing α-syn oligomerization and consequent amplification of the fibrillar α-syn (*Fα-syn*) neurotoxicity, eventually resulting in cell death.

tron transport chain complexes of the inner membrane. It was reported that, in addition to complex I (6, 61, 62), complex IV (63) or complexes III and II (60) are also the targets for α-syn. We speculate that other proteins in the mitochondrial intermembrane space might also interact with α-syn. In this case, α-syn translocation into the intermembrane mitochondrial space could have a potentially significant impact on mitochondrial dysfunctions. In neurons or cancer cells with overexpressed α-syn, for example, the mitochondria exhibited a loss of oxidative phosphorylation capacity and enhanced generation of ROS (14, 64). This mechanism (Fig. 8) also explains the co-localization of α-syn with the MOM (10, 19) and with the inner membrane (6) because our data suggest that α-syn may associate with either mitochondrial membrane. Depending on physiological conditions in the cell, such as the total level of monomeric α-syn in the cytosol (6), cytosolic pH (19), MOM lipid composition (especially its cardiolipin and phosphatidylglycerol content (60)), or potential across the MOM (see discussion below), α-syn interaction with VDAC could be involved in regulation of normal mitochondrial respiration through the modulation of VDAC permeability, α-syn-induced mitochondrial dysfunction and enhanced ROS production, or both (Fig. 8).

The restoration of α-syn toxicity by VDAC1 in the yeast *por1*Δ strain on a semirespiratory galactose medium (Fig. 7) supports our conjecture that α-syn-induced mitochondrial dysfunction occurs through modulation of VDAC permeability and/or VDAC-facilitated α-syn translocation. Studies in yeast have demonstrated association of α-syn with the MOM (65). Toxicity of α-syn in the yeast model of PD depends on mitochondrial function and ROS production by mitochondria (66). Mitochondrial dysfunction is the first symptom of α-syn toxic-

ity in the yeast model (67). Strains deleted in the genes essential for mitochondrial function, such as those for cyclophilin D (CPR3), the three isoforms of the adenine-nucleotide translocator (ANT) AAC1/2/3, and POR1 (65, 66), were more resistant to α-syn toxicity than the wild type strain. Taken together, these data suggest that α-syn translocated through VDAC could impair the respiratory chain, causing increased proton leakage and a burst of ROS production. In turn, increased ROS may trigger α-syn oxidation, inducing α-syn aggregation in the cytosol and the subsequent association of aggregated α-syn with the MOM (Fig. 8). This sequence of events leads to mitochondrial dysfunction and eventually to cell death (7, 14). In this case, interaction of monomeric α-syn with VDAC would amplify the proposed effect of oligomeric or fibrillar α-syn (Fα-syn in Fig. 8) on mitochondrial fragmentation, ROS production, and enhanced neurotoxicity (7, 14).

Recent data on VDAC and α-syn co-immunoprecipitation (9, 20, 68) provide strong biochemical evidence on the interaction of these two proteins in mutant α-syn transgenic mice and support our functional findings. However, in all of these studies, binding of α-syn to VDAC is interpreted as the effect of α-syn on the mitochondrial permeability transition (PT) pore based on the assumption that VDAC is a part of the PT pore. The recent genetic data obtained by several independent groups had unambiguously shown that VDAC is not a part of the PT pore (*e.g.* see Ref. 69 for a review addressing this controversy). The effect of yeast depletion of ANT, another putative component of the PT pore located in the mitochondrial inner membrane, or depletion of VDAC on α-syn toxicity was also discussed exclusively from the point of view of the α-syn effect on the PT pore (65). Again, genetic studies have seriously challenged the notion that ANT is a part of the PT pore (70). Instead, the latest studies have demonstrated that the mysterious PT pore consists of FOF1 ATP synthase and is regulated by matrix cyclophilin D and cyclosporine (71, 72). None of the previous papers discussed how α-syn could access the inner membrane from the cytosol to interact with the putative PT pore component in the inner membrane (ANT) or even with cyclophilin D at the matrix side of the inner membrane. Importantly, our conclusions do not contradict these data but give instead a different explanation by offering a mechanism by which α-syn regulates ATP/ADP flux through VDAC and translocates across the MOM (Fig. 8). According to our model, in order to reach proteins in the mitochondrial inner membrane, including those that compose the PT pore, α-syn first must cross the MOM through VDAC.

Extrapolation of the equilibrium constant to zero voltage gives an estimated K_{eq} of ~0.1 mM^{-1} (Fig. 2*B*). This leads to IC_{50} concentration of about 10 mM, which is significantly higher than the tens of μM estimates for α-syn concentration under physiological conditions in the brain (53, 73). However, bulk cytosolic concentration could be very different from the local concentration at the MOM surface. Keeping in mind that MOM could contain up to 20% of the negatively charged lipids (74) and that α-syn is known to preferentially bind to the negatively charged lipids (16, 55), the local concentration of α-syn could be significantly higher than that in bulk.

In addition, interaction of α-syn with VDAC is highly voltage-dependent. Therefore, at 10–20 mV, IC_{50} of α-syn-VDAC binding is in the range of 3–100 μM (Fig. 2*B*), which is already physiologically relevant. This immediately raises a question about the potential across the MOM *in vivo*, which is usually believed to be close to zero due to the presence of VDAC pores in the MOM. The actual potential across the MOM, including its possible variations with the mitochondrial state, is still a subject of ongoing debate (21). The estimates for the voltage span from 10 mV (75) to as high as 46 mV (76). Depending on α-syn concentration, which might reach ~20 μM in synaptic terminals (77), a 10-mV potential could be enough to promote a significant α-syn binding to VDAC (Fig. 2*B*). By contrast, translocation of α-syn through VDAC requires relatively high voltages of more than 40 mV, which may seem to be unrealistically high for the potential across the MOM. Interestingly, a recently published model (41) suggests that a VDAC complex with hexokinase is a generator of the potential across the MOM with the Gibbs free energy of kinase reactions being used as a driving force. In the framework of this model, the estimated MOM potential is as high as 50 mV, negative at the cytoplasmic side of the MOM. Whatever the MOM potential, it is important to note that α-syn translocation through VDAC, which requires relatively large voltages under the grossly simplified conditions of our reconstitution experiments, may occur much more readily in the crowded, compartmentalized cell environment and in the presence of different chaperons.

Conclusions

Using the channel reconstitution technique, we have demonstrated the existence of a functional interaction between α-syn and VDAC that suggests a previously unknown mechanism of MOM permeability regulation. Our data indicate that α-syn is able to both block VDAC in a concentration- and voltage-dependent manner and translocate via this channel across the MOM. We have also explored a yeast model of PD and shown that α-syn toxicity in yeast depends on VDAC, thus supporting our *in vitro* results. Based on these findings, we believe that our study reveals the evasive physiological and pathophysiological roles for monomeric α-syn and reconciles previous observations of various α-syn effects on mitochondrial bioenergetics.

Author Contributions—T. K. R., P. A. G., and S. M. B. initiated the project. T. K. R., P. A. G., O. P., and S. M. B. designed all experiments, performed data analysis, and wrote the manuscript. T. K. R., P. A. G., and O. P. performed experiments. D. P. H. performed data analysis. T. L. Y. and J. C. L. purified and characterized proteins. D. P. H., J. C. L., and C. C. P. contributed to manuscript writing. All authors reviewed the results and approved the final version of the manuscript.

Acknowledgment—Certain commercial materials, equipment, and instruments are identified in this work to describe the experimental procedure as completely as possible. In no case does such an identification imply a recommendation or endorsement by NIST, nor does it imply that the materials, equipment, or instrument identified are necessarily the best available for the purpose.

References

1. Vila, M., Ramonet, D., and Perier, C. (2008) Mitochondrial alterations in Parkinson's disease: new clues. *J. Neurochem.* **107,** 317–328
2. Federico, A., Cardaioli, E., Da Pozzo, P., Formichi, P., Gallus, G. N., and Radi, E. (2012) Mitochondria, oxidative stress and neurodegeneration. *J. Neurol. Sci.* **322,** 254–262
3. Nakamura, K., Nemani, V. M., Azarbal, F., Skibinski, G., Levy, J. M., Egami, K., Munishkina, L., Zhang, J., Gardner, B., Wakabayashi, J., Sesaki, H., Cheng, Y., Finkbeiner, S., Nussbaum, R. L., Masliah, E., and Edwards, R. H. (2011) Direct membrane association drives mitochondrial fission by the Parkinson disease-associated protein α-synuclein. *J. Biol. Chem.* **286,** 20710–20726
4. Spillantini, M. G., Schmidt, M. L., Lee, V. M. Y., Trojanowski, J. Q., Jakes, R., and Goedert, M. (1997) α-Synuclein in Lewy bodies. *Nature* **388,** 839–840
5. Goedert, M., Jakes, R., Anthony Crowther, R., and Grazia Spillantini, M. (2001) Parkinson's disease, dementia with Lewy bodies, and multiple system atrophy as α-synucleinopathies. *Methods Mol. Med.* **62,** 33–59
6. Devi, L., Raghavendran, V., Prabhu, B. M., Avadhani, N. G., and Anandatheerthavarada, H. K. (2008) Mitochondrial import and accumulation of α-synuclein impair complex I in human dopaminergic neuronal cultures and Parkinson disease brain. *J. Biol. Chem.* **283,** 9089–9100
7. Nakamura, K. (2013) α-Synuclein and mitochondria: partners in crime? *Neurotherapeutics* **10,** 391–399
8. Banerjee, K., Sinha, M., Pham Cle, L., Jana, S., Chanda, D., Cappai, R., and Chakrabarti, S. (2010) α-Synuclein induced membrane depolarization and loss of phosphorylation capacity of isolated rat brain mitochondria: implications in Parkinson's disease. *FEBS Lett.* **584,** 1571–1576
9. Martin, L. J., Semenkow, S., Hanaford, A., and Wong, M. (2014) The mitochondrial permeability transition pore regulates Parkinson's disease development in mutant α-synuclein transgenic mice. *Neurobiol. Aging* **35,** 1132–1152
10. Li, W. W., Yang, R., Guo, J. C., Ren, H. M., Zha, X. L., Cheng, J. S., and Cai, D. F. (2007) Localization of α-synuclein to mitochondria within midbrain of mice. *Neuroreport* **18,** 1543–1546
11. Polymeropoulos, M. H., Lavedan, C., Leroy, E., Ide, S. E., Dehejia, A., Dutra, A., Pike, B., Root, H., Rubenstein, J., Boyer, R., Stenroos, E. S., Chandrasekharappa, S., Athanassiadou, A., Papapetropoulos, T., Johnson, W. G., Lazzarini, A. M., Duvoisin, R. C., Di Iorio, G., Golbe, L. I., and Nussbaum, R. L. (1997) Mutation in the α-synuclein gene identified in families with Parkinson's disease. *Science* **276,** 2045–2047
12. Singleton, A. B., Farrer, M., Johnson, J., Singleton, A., Hague, S., Kachergus, J., Hulihan, M., Peuralinna, T., Dutra, A., Nussbaum, R., Lincoln, S., Crawley, A., Hanson, M., Maraganore, D., Adler, C., Cookson, M. R., Muenter, M., Baptista, M., Miller, D., Blancato, J., Hardy, J., and Gwinn-Hardy, K. (2003) α-Synuclein locus triplication causes Parkinson's disease. *Science* **302,** 841–841
13. Proukakis, C., Dudzik, C. G., Brier, T., MacKay, D. S., Cooper, J. M., Millhauser, G. L., Houlden, H., and Schapira, A. H. (2013) A novel α-synuclein missense mutation in Parkinson disease. *Neurology* **80,** 1062–1064
14. Rochet, J. C., Hay, B. A., and Guo, M. (2012) Molecular insights into Parkinson's disease. *Prog. Mol. Biol. Transl. Sci.* **107,** 125–188
15. Weinreb, P. H., Zhen, W., Poon, A. W., Conway, K. A., and Lansbury, P. T., Jr. (1996) NACP, a protein implicated in Alzheimer's disease and learning, is natively unfolded. *Biochemistry* **35,** 13709–13715
16. Pfefferkorn, C. M., Jiang, Z., and Lee, J. C. (2012) Biophysics of α-synuclein membrane interactions. *Biochim. Biophys. Acta* **1818,** 162–171
17. Nakamura, K., Nemani, V. M., Wallender, E. K., Kaehlcke, K., Ott, M., and Edwards, R. H. (2008) Optical reporters for the conformation of α-synuclein reveal a specific interaction with mitochondria. *J. Neurosci.* **28,** 12305–12317
18. Robotta, M., Gerding, H. R., Vogel, A., Hauser, K., Schildknecht, S., Karreman, C., Leist, M., Subramaniam, V., and Drescher, M. (2014) α-Synuclein binds to the inner membrane of mitochondria in an α-helical conformation. *Chembiochem* **15,** 2499–2502
19. Cole, N. B., Dieuliis, D., Leo, P., Mitchell, D. C., and Nussbaum, R. L. (2008) Mitochondrial translocation of α-synuclein is promoted by intracellular acidification. *Exp. Cell Res.* **314,** 2076–2089
20. Lu, L., Zhang, C., Cai, Q., Lu, Q., Duan, C., Zhu, Y., and Yang, H. (2013) Voltage-dependent anion channel involved in the α-synuclein-induced dopaminergic neuron toxicity in rats. *Acta Biochim. Biophys. Sin.* **45,** 170–178
21. Colombini, M. (2004) VDAC: the channel at the interface between mitochondria and the cytosol. *Mol. Cell Biochem.* **256,** 107–115
22. Lemasters, J. J., and Holmuhamedov, E. (2006) Voltage-dependent anion channel (VDAC) as mitochondrial governator: thinking outside the box. *Biochim. Biophys. Acta* **1762,** 181–190
23. Rostovtseva, T. K., Tan, W., and Colombini, M. (2005) On the role of VDAC in apoptosis: fact and fiction. *J. Bioenerg. Biomembr.* **37,** 129–142
24. Shoshan-Barmatz, V., and Gincel, D. (2003) The voltage-dependent anion channel: characterization, modulation, and role in mitochondrial function in cell life and death. *Cell Biochem. Biophys.* **39,** 279–292
25. Shoshan-Barmatz, V., and Ben-Hail, D. (2012) VDAC, a multi-functional mitochondrial protein as a pharmacological target. *Mitochondrion* **12,** 24–34
26. Maldonado, E. N., and Lemasters, J. J. (2012) Warburg revisited: regulation of mitochondrial metabolism by voltage-dependent anion channels in cancer cells. *J. Pharmacol. Exp. Ther.* **342,** 637–641
27. Rostovtseva, T. K., and Bezrukov, S. M. (2012) VDAC inhibition by tubulin and its physiological implications. *Biochim. Biophys. Acta* **1818,** 1526–1535
28. Shoshan-Barmatz, V., De Pinto, V., Zweckstetter, M., Raviv, Z., Keinan, N., and Arbel, N. (2010) VDAC, a multi-functional mitochondrial protein regulating cell life and death. *Mol. Aspects Med.* **31,** 227–285
29. Rostovtseva, T., and Colombini, M. (1996) ATP flux is controlled by a voltage-gated channel from the mitochondrial outer membrane. *J. Biol. Chem.* **271,** 28006–28008
30. Pfefferkorn, C. M., and Lee, J. C. (2010) Tryptophan probes at the α-synuclein and membrane interface. *J. Phys. Chem. B* **114,** 4615–4622
31. Gurnev, P. A., Yap, T. L., Pfefferkorn, C. M., Rostovtseva, T. K., Berezhkovskii, A. M., Lee, J. C., Parsegian, V. A., and Bezrukov, S. M. (2014) α-Synuclein lipid-dependent membrane binding and translocation through the α-hemolysin channel. *Biophys. J.* **106,** 556–565
32. Rostovtseva, T. K., Kazemi, N., Weinrich, M., and Bezrukov, S. M. (2006) Voltage gating of VDAC is regulated by nonlamellar lipids of mitochondrial membranes. *J. Biol. Chem.* **281,** 37496–37506
33. Sigworth, F. J., and Sine, S. M. (1987) Data transformations for improved display and fitting of single-channel dwell time histograms. *Biophys. J.* **52,** 1047–1054
34. Büttner, S., Faes, L., Reichelt, W. N., Broeskamp, F., Habernig, L., Benke, S., Kourtis, N., Ruli, D., Carmona-Gutierrez, D., Eisenberg, T., D'hooge, P., Ghillebert, R., Franssens, V., Harger, A., Pieber, T. R., Freudenberger, P., Kroemer, G., Sigrist, S. J., Winderickx, J., Callewaert, G., Tavernarakis, N., and Madeo, F. (2013) The Ca^{2+}/Mn^{2+} ion-pump PMR1 links elevation of cytosolic Ca^{2+} levels to α-synuclein toxicity in Parkinson's disease models. *Cell Death Differ.* **20,** 465–477
35. De Pinto, V., Guarino, F., Guarnera, A., Messina, A., Reina, S., Tomasello, F. M., Palermo, V., and Mazzoni, C. (2010) Characterization of human VDAC isoforms: a peculiar function for VDAC3? *Biochim. Biophys. Acta* **1797,** 1268–1275
36. Sherman, F. (1991) Getting started with yeast. *Methods Enzymol.* **194,** 3–21
37. Ciaccioli, G., Martins, A., Rodrigues, C., Vieira, H., and Calado, P. (2013) A powerful yeast model to investigate the synergistic interaction of α-synuclein and τ in neurodegeneration. *PLoS One* **8,** e55848
38. Gurnev, P. A., Rostovtseva, T. K., and Bezrukov, S. M. (2011) Tubulin-blocked state of VDAC studied by polymer and ATP partitioning. *FEBS Lett.* **585,** 2363–2366
39. Colombini, M. (1989) Voltage gating in the mitochondrial channel, VDAC. *J. Membr. Biol.* **111,** 103–111
40. Carneiro, C. M., Merzlyak, P. G., Yuldasheva, L. N., Silva, L. G., Thinnes, F. P., and Krasilnikov, O. V. (2003) Probing the volume changes during voltage gating of Porin 31BM channel with nonelectrolyte polymers. *Biochim. Biophys. Acta* **1612,** 144–153
41. Lemeshko, V. V. (2014) VDAC electronics: 1. VDAC-hexo(gluco)kinase

generator of the mitochondrial outer membrane potential. *Biochim. Biophys. Acta* **1838,** 1362–1371
42. Rostovtseva, T., and Colombini, M. (1997) VDAC channels mediate and gate the flow of ATP: implications for the regulation of mitochondrial function. *Biophys. J.* **72,** 1954–1962
43. Woodhull, A. M. (1973) Ionic blockage of sodium channels in nerve. *J. Gen. Physiol.* **61,** 687–708
44. Blaustein, R. O., Lea, E. J., and Finkelstein, A. (1990) Voltage-dependent block of anthrax toxin channels in planar phospholipid bilayer membranes by symmetric tetraalkylammonium ions. Single-channel analysis. *J. Gen. Physiol.* **96,** 921–942
45. Bezrukov, S. M., Krasilnikov, O. V., Yuldasheva, L. N., Berezhkovskii, A. M., and Rodrigues, C. G. (2004) Field-dependent effect of crown ether (18-crown-6) on ionic conductance of α-hemolysin channels. *Biophys. J.* **87,** 3162–3171
46. Movileanu, L., Schmittschmitt, J. P., Scholtz, J. M., and Bayley, H. (2005) Interactions of peptides with a protein pore. *Biophys. J.* **89,** 1030–1045
47. Wolfe, A. J., Mohammad, M. M., Cheley, S., Bayley, H., and Movileanu, L. (2007) Catalyzing the translocation of polypeptides through attractive interactions. *J. Am. Chem. Soc.* **129,** 14034–14041
48. Krüger, R., Kuhn, W., Müller, T., Woitalla, D., Graeber, M., Kösel, S., Przuntek, H., Epplen, J. T., Schöls, L., and Riess, O. (1998) Ala30Pro mutation in the gene encoding α-synuclein in Parkinson's disease. *Nat. Genet.* **18,** 106–108
49. Zakharov, S. D., Hulleman, J. D., Dutseva, E. A., Antonenko, Y. N., Rochet, J. C., and Cramer, W. A. (2007) Helical α-synuclein forms highly conductive ion channels. *Biochemistry* **46,** 14369–14379
50. Rostovtseva, T. K., Sheldon, K. L., Hassanzadeh, E., Monge, C., Saks, V., Bezrukov, S. M., and Sackett, D. L. (2008) Tubulin binding blocks mitochondrial voltage-dependent anion channel and regulates respiration. *Proc. Natl. Acad. Sci. U.S.A.* **105,** 18746–18751
51. Maglia, G., Restrepo, M. R., Mikhailova, E., and Bayley, H. (2008) Enhanced translocation of single DNA molecules through α-hemolysin nanopores by manipulation of internal charge. *Proc. Natl. Acad. Sci. U.S.A.* **105,** 19720–19725
52. Ujwal, R., Cascio, D., Colletier, J.-P., Faham, S., Zhang, J., Toro, L., Ping, P., and Abramson, J. (2008) The crystal structure of mouse VDAC1 at 2.3 Å resolution reveals mechanistic insights into metabolite gating. *Proc. Natl. Acad. Sci. U.S.A.* **105,** 17742–17747
53. Cremades, N., Cohen, S. I., Deas, E., Abramov, A. Y., Chen, A. Y., Orte, A., Sandal, M., Clarke, R. W., Dunne, P., Aprile, F. A., Bertoncini, C. W., Wood, N. W., Knowles, T. P., Dobson, C. M., and Klenerman, D. (2012) Direct observation of the interconversion of normal and toxic forms of α-synuclein. *Cell* **149,** 1048–1059
54. Serpell, L. C., Berriman, J., Jakes, R., Goedert, M., and Crowther, R. A. (2000) Fiber diffraction of synthetic α-synuclein filaments shows amyloid-like cross-β conformation. *Proc. Natl. Acad. Sci. U.S.A.* **97,** 4897–4902
55. Davidson, W. S., Jonas, A., Clayton, D. F., and George, J. M. (1998) Stabilization of α-synuclein secondary structure upon binding to synthetic membranes. *J. Biol. Chem.* **273,** 9443–9449
56. Conway, K. A., Harper, J. D., and Lansbury, P. T. (1998) Accelerated *in vitro* fibril formation by a mutant α-synuclein linked to early-onset Parkinson disease. *Nat. Med.* **4,** 1318–1320
57. Murray, I. V., Giasson, B. I., Quinn, S. M., Koppaka, V., Axelsen, P. H., Ischiropoulos, H., Trojanowski, J. Q., and Lee, V. M. (2003) Role of α-synuclein carboxy-terminus on fibril formation *in vitro*. *Biochemistry* **42,** 8530–8540
58. Crowther, R. A., Jakes, R., Spillantini, M. G., and Goedert, M. (1998) Synthetic filaments assembled from C-terminally truncated α-synuclein. *FEBS Lett.* **436,** 309–312
59. Maldonado, E. N., Patnaik, J., Mullins, M. R., and Lemasters, J. J. (2010) Free tubulin modulates mitochondrial membrane potential in cancer cells. *Cancer Res.* **70,** 10192–10201
60. Ellis, C. E., Murphy, E. J., Mitchell, D. C., Golovko, M. Y., Scaglia, F., Barceló-Coblijn, G. C., and Nussbaum, R. L. (2005) Mitochondrial lipid abnormality and electron transport chain impairment in mice lacking α-synuclein. *Mol. Cell. Biol.* **25,** 10190–10201
61. Luth, E. S., Stavrovskaya, I. G., Bartels, T., Kristal, B. S., and Selkoe, D. J. (2014) Soluble, prefibrillar α-synuclein oligomers promote complex I-dependent, Ca^{2+}-induced mitochondrial dysfunction. *J. Biol. Chem.* **289,** 21490–21507
62. Liu, G., Zhang, C., Yin, J., Li, X., Cheng, F., Li, Y., Yang, H., Uéda, K., Chan, P., and Yu, S. (2009) α-Synuclein is differentially expressed in mitochondria from different rat brain regions and dose-dependently down-regulates complex I activity. *Neurosci. Lett.* **454,** 187–192
63. Elkon, H., Don, J., Melamed, E., Ziv, I., Shirvan, A., and Offen, D. (2002) Mutant and wild-type α-synuclein interact with mitochondrial cytochrome *c* oxidase. *J. Mol. Neurosci.* **18,** 229–238
64. Junn, E., and Mouradian, M. M. (2002) Human α-synuclein over-expression increases intracellular reactive oxygen species levels and susceptibility to dopamine. *Neurosci. Lett.* **320,** 146–150
65. Büttner, S., Habernig, L., Broeskamp, F., Ruli, D., Vögtle, F. N., Vlachos, M., Macchi, F., Küttner, V., Carmona-Gutierrez, D., Eisenberg, T., Ring, J., Markaki, M., Taskin, A. A., Benke, S., Ruckenstuhl, C., Braun, R., Van den Haute, C., Bammens, T., van der Perren, A., Fröhlich, K. U., Winderickx, J., Kroemer, G., Baekelandt, V., Tavernarakis, N., Kovacs, G. G., Dengjel, J., Meisinger, C., Sigrist, S. J., and Madeo, F. (2013) Endonuclease G mediates α-synuclein cytotoxicity during Parkinson's disease. *EMBO J.* **32,** 3041–3054
66. Büttner, S., Bitto, A., Ring, J., Augsten, M., Zabrocki, P., Eisenberg, T., Jungwirth, H., Hutter, S., Carmona-Gutierrez, D., Kroemer, G., Winderickx, J., and Madeo, F. (2008) Functional mitochondria are required for α-synuclein toxicity in aging yeast. *J. Biol. Chem.* **283,** 7554–7560
67. Su, L. J., Auluck, P. K., Outeiro, T. F., Yeger-Lotem, E., Kritzer, J. A., Tardiff, D. F., Strathearn, K. E., Liu, F., Cao, S., Hamamichi, S., Hill, K. J., Caldwell, K. A., Bell, G. W., Fraenkel, E., Cooper, A. A., Caldwell, G. A., McCaffery, J. M., Rochet, J. C., and Lindquist, S. (2010) Compounds from an unbiased chemical screen reverse both ER-to-Golgi trafficking defects and mitochondrial dysfunction in Parkinson's disease models. *Dis. Model. Mech.* **3,** 194–208
68. Shen, J., Du, T., Wang, X., Duan, C., Gao, G., Zhang, J., Lu, L., and Yang, H. (2014) α-Synuclein amino terminus regulates mitochondrial membrane permeability. *Brain Res.* **1591,** 14–26
69. McCommis, K. S., and Baines, C. P. (2012) The role of VDAC in cell death: friend or foe? *Biochim. Biophys. Acta* **1818,** 1444–1450
70. Kokoszka, J. E., Waymire, K. G., Levy, S. E., Sligh, J. E., Cai, J., Jones, D. P., MacGregor, G. R., and Wallace, D. C. (2004) The ADP/ATP translocator is not essential for the mitochondrial permeability transition pore. *Nature* **427,** 461–465
71. Alavian, K. N., Dworetzky, S. I., Bonanni, L., Zhang, P., Sacchetti, S., Li, H., Signore, A. P., Smith, P. J., Gribkoff, V. K., and Jonas, E. A. (2015) The mitochondrial complex V-associated large-conductance inner membrane current is regulated by cyclosporine and dexpramipexole. *Mol. Pharmacol.* **87,** 1–8
72. Giorgio, V., von Stockum, S., Antoniel, M., Fabbro, A., Fogolari, F., Forte, M., Glick, G. D., Petronilli, V., Zoratti, M., Szabó, I., Lippe, G., and Bernardi, P. (2013) Dimers of mitochondrial ATP synthase form the permeability transition pore. *Proc. Natl. Acad. Sci. U.S.A.* **110,** 5887–5892
73. Iwai, A., Masliah, E., Yoshimoto, M., Ge, N., Flanagan, L., de Silva, H. A., Kittel, A., and Saitoh, T. (1995) The precursor protein of non-Aβ component of Alzheimer's disease amyloid is a presynaptic protein of the central nervous system. *Neuron* **14,** 467–475
74. Daum, G. (1985) Lipids of mitochondria. *Biochim. Biophys. Acta* **822,** 1–42
75. Lemeshko, V. V. (2006) Theoretical evaluation of a possible nature of the outer membrane potential of mitochondria. *Eur. Biophys. J.* **36,** 57–66
76. Porcelli, A. M., Ghelli, A., Zanna, C., Pinton, P., Rizzuto, R., and Rugolo, M. (2005) pH difference across the outer mitochondrial membrane measured with a green fluorescent protein mutant. *Biochem. Biophys. Res. Commun.* **326,** 799–804
77. Wilhelm, B. G., Mandad, S., Truckenbrodt, S., Kröhnert, K., Schäfer, C., Rammner, B., Koo, S. J., Classen, G. A., Krauss, M., Haucke, V., Urlaub, H., and Rizzoli, S. O. (2014) Composition of isolated synaptic boutons reveals the amounts of vesicle trafficking proteins. *Science* **344,** 1023–1028